Tri-periodic fully 3D analytic solutions for the Navier-Stokes equations

By Matteo Antuono†

CNR-INM, Via di Vallerano 139, 00128 Rome, Italy

(Received 10 February 2020)

Unsteady tri-periodic laminar solutions of the Navier-Stokes equations are derived. In particular, these represent fully three-dimensional flows, since all the velocity components depend non-trivially on all three coordinate directions. We show that they belong to the class of Beltrami's flows and that can be gathered in two distinct solutions characterized by positive and negative helicity respectively. These can be regarded as an extension in three-dimensions of the bi-periodic vortex solution of Taylor (1923). Their use as benchmarks for checking the accuracy of 3D numerical codes and /or studying the onset of turbulence is suggested.

1. Introduction

In the last decade, the growing computational power has led to an increasing number of numerical applications concerning three-dimensional problems in fluid-dynamics. The validation of codes for such a kind of simulations is, however, difficult due to the complexity of fully three-dimensional fluid motions. With respect to this, comparisons with experiments would be desirable, even though these are not always available or may be difficult to handle because of a number of issues concerning the experimental measurements. In this context, the possibility of checking numerical codes against analytical solutions represents a considerable advantage since this allows for a complete control of the physical quantities of interest and, from a numerical point of view, it makes the assignment of boundary/initial conditions very easy. Unfortunately, the availability of fully three-dimensional solutions for incompressible viscous fluids is very limited. With respect to this, a summary of analytic solutions can be found, for example, in Wang (1989) and Langlois & Deville (2014).

The aim of the present work is, therefore, to give a further contribution in this direction. Specifically, we provide a class of unsteady tri-periodic fully three-dimensional solutions of the Navier-Stokes equations, basing on the work of Ethier-Ross & Steinman (1999). These correspond to laminar flows and can be gathered in two distinct solutions characterized by positive and negative helicity respectively. In particular, they both belong to the class of Beltrami flows (where vorticity and velocity fields are parallel) and can be regarded as extensions in three-dimensions of the well-known vortex solution by Taylor (1923).

The benchmarking of numerical schemes is, obviously, the most straightforward application of the proposed analytical results. The periodicity of these solutions (and the consequent absence of boundaries) makes them particularly simple to use. In any case, this does not run out all possible applications of the proposed outcomes. Since such solutions represent the free evolution of rotational three-dimensional patterns, they can be adopted to study the onset of instabilities and the possible transition to turbulence in three-dimensional flows. This was, in fact, the original idea at the basis of the work by Taylor & Green (1937) where the initial evolution of a viscous

† Email address for correspondence: matteo.antuono@cnr.it

fluid from a particular three-dimensional initial condition was studied. Such an initial condition was related to the bi-periodic vortex pattern described in Taylor (1923) of which, in some sense, it represented an extension in 3D. At the present time, the above-mentioned approach is very common when dealing with numerical simulations of turbulence in three-dimensions: the strategy is to initialize the computations through a three-dimensional divergence-free velocity field that extends the two-dimensional vortex pattern and, then, study the subsequent evolution to turbulence (see Brachet et al. (1983), Berselli (2005), Drikakis et al. (2007)). Incidentally, we highlight that in many works the adopted three-dimensional initial condition is characterized by a null component in one direction (see, for example, Goldstein (1940), Orszag (1974), Sharma & Sengupta (2019)) and this implies longer times to reach a fully-developed homogeneous and isotropic turbulent flow. Such an issue may be easily overcome by using the proposed fully three-dimensional solutions. Similarly to the works of Di Mascio et al. (2017) and Sengupta et al. (2018a) where the stability of the two-dimensional solution by Taylor (1923) was studied, the proposed solutions may represent a further tool for the inspection of the stability of three-dimensional flows and their transition to turbulence.

2. Solution structure

Here we briefly recall the solution structure described in Ethier-Ross & Steinman (1999). First, we introduce the Navier-Stokes equations for incompressible fluids:

$$\begin{cases} \nabla \cdot \boldsymbol{u} \;=\; 0\,, \\ \\ \dfrac{\partial \boldsymbol{u}}{\partial t} \;+\; (\boldsymbol{u}\cdot\nabla)\,\boldsymbol{u} \;=\; -\dfrac{\nabla p}{\rho} \;+\; \nu\,\Delta \boldsymbol{u}\,, \end{cases} \tag{2.1}$$

where $\boldsymbol{u} = (u, v, w)$ is the velocity vector, p is the pressure field, ρ is the density (constant) and ν is the kinematic viscosity. The class of solutions described in Ethier-Ross & Steinman (1999) are obtained by following an approach similar to that adopted for deriving the Taylor vortex solution (see Taylor (1923)). Specifically, the strategy is to look for a divergence-free velocity field such that:

(a) the unsteady terms (namely, $\partial \boldsymbol{u}/\partial t$) balance the viscous terms in the momentum equations,

(b) the advective terms $(\boldsymbol{u}\cdot\nabla)\,\boldsymbol{u}$ can be expressed as the gradient of a scalar function, that is $(\boldsymbol{u}\cdot\nabla)\,\boldsymbol{u} = \nabla H$ where H is defined apart from an unessential constant value.

Since $\boldsymbol{u}$ has to be divergence-free, the velocity field can be represented through the stream-function $\boldsymbol{\psi}$ such that $\boldsymbol{u} = \nabla\times\boldsymbol{\psi}$. Under the hypotheses above, the continuity equation is identically satisfied and the momentum equation can be rearranged as follows:

$$\nabla \times \left[\frac{\partial \boldsymbol{\psi}}{\partial t} \;-\; \nu\,\Delta \boldsymbol{\psi} \right] \;=\; -\,\nabla \left[\frac{p}{\rho} \;+\; H \right]. \tag{2.2}$$

The approach followed by Taylor (1923) and later by Ethier-Ross & Steinman (1999) is to decompose the divergence-free field and the gradient field and obtain two separate equations:

$$\frac{\partial \boldsymbol{\psi}}{\partial t} \;=\; \nu\,\Delta \boldsymbol{\psi}\,, \qquad \frac{p}{\rho} \;+\; H \;=\; \text{constant}\,. \tag{2.3}$$

The idea above is of fundamental importance for the derivation of the analytical solutions, since it allows one to "move" all the nonlinear contributions to the pressure field (through the term H) and obtain a linear equation for the stream function $\boldsymbol{\psi}$. Incidentally, we observe that the second

relation in the equation (2.3) means that the mechanical energy, namely $E_m = p/\rho + H$, maintains constant during the flow evolution. For what concerns the first equation in (2.3), the following separation of variables is adopted:

$$\boldsymbol{\psi}(\boldsymbol{x}, t) = \boldsymbol{\Psi}(\boldsymbol{x})\, T(\tau)\,, \tag{2.4}$$

where $\boldsymbol{\Psi} = \left(\Psi_{yz}, \Psi_{zx}, \Psi_{xy}\right)$ and $\tau = \nu\, t$. Then, it follows:

$$\frac{\mathrm{d}T}{\mathrm{d}\tau} = \lambda\, T\,, \qquad \Delta\boldsymbol{\Psi} = \lambda\, \boldsymbol{\Psi}\,, \tag{2.5}$$

where $\lambda \in \mathbb{C}$. The first equation above gives $T(\tau) = \exp(\lambda\, \tau)$, implying that $\Re(\lambda) \leq 0$ is required in order to find bounded solutions for $\tau > 0$. To satisfy the second equation in (2.5), Ethier-Ross & Steinman (1999) adopted the decomposition below:

$$\Psi_{yz} = f(y)\, g(z)\, h(x)\,, \quad \Psi_{zx} = f(z)\, g(x)\, h(y)\,, \quad \Psi_{xy} = f(x)\, g(y)\, h(z)\,. \tag{2.6}$$

where f, g and h have to satisfy the following relations:

$$\ddot{f} = a^2\, f\,, \quad \ddot{g} = b^2\, g\,, \quad \ddot{h} = c^2\, h\,, \tag{2.7}$$

with $\lambda = a^2 + b^2 + c^2$ and $a, b, c \in \mathbb{C}$.

The last condition to fulfil is the requirement that $(\boldsymbol{u} \cdot \nabla)\, \boldsymbol{u}$ is a gradient. This is equivalent to impose $\nabla \times [(\boldsymbol{u} \cdot \nabla)\, \boldsymbol{u}] = 0$. Using standard algebra, the latter condition corresponds to:

$$\nabla \times [\, \boldsymbol{u} \times (\nabla \times \boldsymbol{u})\,] = 0\,. \tag{2.8}$$

Flows satisfying the above equation are called generalized Beltrami flows. As a particular case, flows that satisfy the equation (2.8) with $\boldsymbol{u} \times (\nabla \times \boldsymbol{u}) = 0$ are said to be Beltrami flows. The latter are characterized by a vorticity field which is always parallel to the velocity vector. Incidentally, we observe that Beltrami flows can never represent planar or axisymmetric motions, since in these latter cases the vorticity is always perpendicular to the velocity field. The role played by velocity, vorticity and their scalar product (namely helicity) is inspected, for example, in Berselli & Cordoba (2009) with specific focus on the regularity of the flow evolution.

2.1. *A brief review of the literature*

Before describing the proposed solutions, we summarize here some of the available results obtained through the procedure described in the previous section.

As observed in Ethier-Ross & Steinman (1999), the Taylor's 2D solution is obtained back by setting $\Psi_{yz} = \Psi_{xz} = 0$ and $\Psi_{xy} = f(x)\, g(y)$ (that is $h = 1$). This bi-periodic solution belongs to the generalized Beltrami flows and reads:

$$\begin{cases} u = -\cos(kx)\, \sin(ky)\, e^{-2\nu k^2 t}\,, \\ \\ v = \sin(kx)\, \cos(ky)\, e^{-2\nu k^2 t}\,, \\ \\ p = -\rho\, \dfrac{\cos(2kx) + \cos(2ky)}{4}\, e^{-4\nu k^2 t} \end{cases}$$

where $k = 2\pi/L$ and L is the wave length. Sometimes this is erroneously referred to as Taylor-Green vortex solution but in the original work [i.e., Taylor (1923)] Taylor is the unique author while both Taylor & Green appear in the subsequent paper [namely Taylor & Green (1937)] that is devoted to the analysis of the early stages of the evolution of a viscous fluid from periodic three-dimensional initial conditions.

In their work, Ethier-Ross & Steinman (1999) described a number of original solutions obtained through the procedure illustrated in Section §2. In particular, they considered the cases:

• $a + b + c = 0$ for $a, b, c \in \mathbb{R}$. This choice is, however, not useful for benchmarking because of the unbounded growth in time of the solution ($\Re(\lambda) > 0$),

• $a^2 + b^2 = 0$ and c purely imaginary. In this case, the solution belongs to Beltrami flows and is made of exponentials and sine/cosine functions of the spatial variables while decays exponentially in time ($\Re(\lambda) < 0$).

In any case no one of the motions above is tri-periodic and, consequently, an explicit modelling of the boundary of the computational domain is required for numerical simulations.

On the contrary, a tri-periodic solution obtained by using the approach of Ethier-Ross & Steinman (1999) is described in Barbato et al. (2007). Specifically, this is a Beltrami flow and corresponds to the choice $a = c = 0$ and $b = \imath k$ (namely, $f = h = 1$) and reads:

$$\begin{cases} u = \left[A \sin(kz) + C \cos(ky) \right] e^{-\nu k^2 t}, \\ v = \left[B \sin(kx) + A \cos(kz) \right] e^{-\nu k^2 t}, \\ w = \left[C \sin(ky) + B \cos(kx) \right] e^{-\nu k^2 t}, \\ p = -\rho \left[BC \cos(kx)\sin(ky) + AB \sin(kx)\cos(kz) + AC \sin(kz)\cos(ky) \right] e^{-2\nu k^2 t} \end{cases} \tag{2.9}$$

where A, B and C are arbitrary constants. Incidentally, we observe that this is not a fully 3D motion, since the components of the velocity field do not depend on all the spatial variables (in particular, $u_x = v_y = w_z = 0$).

Finally, we stress that the absence of boundaries in the domain makes periodic solutions particularly suited to study the onset of instabilities in the flow and the subsequent transition to turbulence numerically. Indeed, the fluid is free to evolve and is not influenced by the specific numerical treatment of the boundaries.

3. Tri-periodic fully 3D solutions

Here we look for a tri-periodic fully 3D solution of the form described in Section §2. In particular, we simplify the problem by requiring the same periodicity in the three directions, namely $a = b = c = \imath k$ where k is the wave number and $L = 2\pi/k$ is the wave length. Under these hypotheses, the equation (2.7) gives:

$$f(s) = A \cos(ks) + B \sin(ks), \tag{3.1}$$

$$g(s) = C \cos(ks) + D \sin(ks), \tag{3.2}$$

$$h(s) = E \cos(ks) + F \sin(ks). \tag{3.3}$$

The solution of the equation (2.8) leads to a system of three nonlinear equations for the coefficients A, B, C, D, E, F (see the appendix A for details). After dropping the trivial cases (that is, those leading to a null velocity field), we find two distinct families of solutions:

$$A_{1,2} = (r_{2,1})\, B, \qquad C_{1,2} = (r_{1,2})\, D, \tag{3.4}$$

where the subscripts '1' and '2' indicate the specific family of the solution and:

$$r_1 = \frac{\sqrt{3}\,E - F}{\sqrt{3}\,F + E}, \qquad r_2 = \frac{\sqrt{3}\,E + F}{\sqrt{3}\,F - E}. \tag{3.5}$$

We stress here that these may not be the unique non-trivial choices for the coefficients A, B, C, D, E, F and that further solutions may exist. It is simple to prove that both the families

belong to the class of Beltrami flows and, in particular, the vorticity and velocity fields are linked by the following relation:

$$\boldsymbol{\omega}_{1,2} \;=\; \pm\,\sqrt{3}\,k\,\boldsymbol{u}_{1,2}\,, \tag{3.6}$$

which discriminates the two families according to the sign of the helicity field, namely $\boldsymbol{\omega}\cdot\boldsymbol{u}$. At present, we do not know whether the system reported in the appendix A contains solutions of the general case $\nabla\times[\boldsymbol{u}\times(\nabla\times\boldsymbol{u})]=0$.

Before proceeding to the analysis, we highlight that, since the pressure gradient balances the nonlinear advective terms in the momentum equation and the vorticity is parallel to the velocity field, it immediately follows:

$$\frac{\nabla p}{\rho} \;=\; -\,(\boldsymbol{u}\cdot\nabla)\,\boldsymbol{u} \;=\; -\left[\,\nabla\left(\frac{\|\boldsymbol{u}\|^2}{2}\right)+\,\boldsymbol{\omega}\times\boldsymbol{u}\,\right] \;=\; -\,\nabla\left(\frac{\|\boldsymbol{u}\|^2}{2}\right), \tag{3.7}$$

which implies:

$$p_{1,2} \;=\; p_0 \;-\; \rho\,\frac{\|\boldsymbol{u}_{1,2}\|^2}{2}\,, \tag{3.8}$$

where p_0 is a generic constant (hereinafter set equal to zero). Then, the knowledge of the velocity field immediately allows for the derivation of both the pressure and vorticity fields. Incidentally, we observe that the vortex stretching term is proportional to the gradient of the kinetic energy. Indeed, from the equation (3.6), we find:

$$\mathscr{V}^{S}_{1,2} \;=\; (\boldsymbol{\omega}_{1,2}\cdot\nabla)\,\boldsymbol{u}_{1,2} \;=\; \pm\,\sqrt{3}\,k\,(\boldsymbol{u}_{1,2}\cdot\nabla)\,\boldsymbol{u}_{1,2} \;=\; \pm\,\sqrt{3}\,k\,\nabla\left(\frac{\|\boldsymbol{u}_{1,2}\|^2}{2}\right), \tag{3.9}$$

where the last equality is obtained following the derivation of the equation (3.7). Then, the extrema of the kinetic energy field correspond to the points where the vortex stretching term is null.

3.1. *One-parameter families*

In the present section we show that the two families of solutions described in the equation (3.4) are actually characterized by just one parameter, namely $R = F/E$. In particular, imposing the kinetic energy of the solution to be finite, it is possible to remove the apparent singularities at $R=\pm 1/\sqrt{3}$ in the equation (3.5), obtaining:

$$\begin{aligned} u_{1,2} = \frac{4\sqrt{2}}{3\sqrt{3}}\,[\,&\sin(kx+\theta_{1,2})\,\cos(ky+\phi_{1,2})\sin(kz+\psi_{1,2}) \\ &-\cos(kz+\theta_{1,2})\,\sin(kx+\phi_{1,2})\sin(ky+\psi_{1,2})\,]\,e^{-3\,\nu k^2 t}\,U_0 \end{aligned} \tag{3.10}$$

$$\begin{aligned} v_{1,2} = \frac{4\sqrt{2}}{3\sqrt{3}}\,[\,&\sin(ky+\theta_{1,2})\,\cos(kz+\phi_{1,2})\sin(kx+\psi_{1,2}) \\ &-\cos(kx+\theta_{1,2})\,\sin(ky+\phi_{1,2})\sin(kz+\psi_{1,2})\,]\,e^{-3\,\nu k^2 t}\,U_0 \end{aligned} \tag{3.11}$$

$$\begin{aligned} w_{1,2} = \frac{4\sqrt{2}}{3\sqrt{3}}\,[\,&\sin(kz+\theta_{1,2})\,\cos(kx+\phi_{1,2})\sin(ky+\psi_{1,2}) \\ &-\cos(ky+\theta_{1,2})\,\sin(kz+\phi_{1,2})\sin(kx+\psi_{1,2})\,]\,e^{-3\,\nu k^2 t}\,U_0 \end{aligned} \tag{3.12}$$

where U_0 is the reference velocity. By construction (see the appendix A), the latter is related to the averaged kinetic energy per unit of mass as below:

$$\overline{\mathscr{E}}(t) \,=\, \frac{1}{L^3}\int_0^L\int_0^L\int_0^L \frac{\|\boldsymbol{u}\|^2}{2}\mathrm{d}x\,\mathrm{d}y\,\mathrm{d}z \,=\, \frac{U_0^2}{2}\,e^{-6\,\nu\,k^2\,t}\,, \tag{3.13}$$

so that $\overline{\mathscr{E}}(0) \,=\, U_0^2/2$ at the initial time. The phases θ_1, ϕ_1 and ψ_1 are given by the following relations:

$$(\sin\theta_1, \cos\theta_1) \,=\, \left(-\frac{\sqrt{3}+R}{2\sqrt{1+R^2}}\,,\, \frac{1-\sqrt{3}R}{2\sqrt{1+R^2}}\right), \tag{3.14}$$

$$(\sin\phi_1, \cos\phi_1) \,=\, \left(\frac{\sqrt{3}-R}{2\sqrt{1+R^2}}\,,\, \frac{1+\sqrt{3}R}{2\sqrt{1+R^2}}\right), \tag{3.15}$$

$$(\sin\psi_1, \cos\psi_1) \,=\, \left(\frac{1}{\sqrt{1+R^2}}\,,\, \frac{R}{\sqrt{1+R^2}}\right). \tag{3.16}$$

Using standard trigonometric identities, we obtain:

$$\Big(\,\sin(\theta_1-\psi_1)\,,\cos(\theta_1-\psi_1)\Big) \,=\, \left(-\frac{1}{2}\,,-\frac{\sqrt{3}}{2}\right)$$

$$\Big(\,\sin(\phi_1-\psi_1)\,,\cos(\phi_1-\psi_1)\Big) \,=\, \left(-\frac{1}{2}\,,+\frac{\sqrt{3}}{2}\right)$$

which lead to:

$$\theta_1 \,=\, \psi_1 \,-\, \frac{5}{6}\,\pi\,, \qquad \phi_1 \,=\, \psi_1 \,-\, \frac{\pi}{6}\,, \qquad \text{where} \quad \psi_1 \,=\, \arccos\left(\frac{R}{\sqrt{1+R^2}}\right). \tag{3.17}$$

For the second family of solutions we find $\theta_2 = \phi_1$, $\phi_2 = \theta_1$ and $\psi_2 = \psi_1 = \psi$ where the symbol ψ is used hereinafter for the sake of the notation.

A deeper insight of the above findings shows that the parameter R (or, equivalently, the angle ψ) corresponds to a translation of the solutions of both the families in the direction $(1, 1, 1)$. From a different perspective, we can represent each family through a reference solution and translate it in the direction $(1, 1, 1)$ through different choices of R (or ψ). In particular, through the translation below:

$$(x', y', z') \,=\, (x, y, z) \,+\, \frac{\psi}{k}\,(1, 1, 1)\,, \tag{3.18}$$

we can rearrange the equations (3.10)-(3.12) for the family '1' into the following reference solution:

$$\frac{u_1}{U_0} \,=\, \frac{4\sqrt{2}}{3\sqrt{3}}\left[\,\sin\!\left(kx'-\frac{5}{6}\pi\right)\cos\!\left(ky'-\frac{\pi}{6}\right)\sin(kz') - \cos\!\left(kz'-\frac{5}{6}\pi\right)\sin\!\left(kx'-\frac{\pi}{6}\right)\sin(ky')\,\right] e^{-3\,\nu\,k^2\,t}$$

$$\frac{v_1}{U_0} \,=\, \frac{4\sqrt{2}}{3\sqrt{3}}\left[\,\sin\!\left(ky'-\frac{5}{6}\pi\right)\cos\!\left(kz'-\frac{\pi}{6}\right)\sin(kx') - \cos\!\left(kx'-\frac{5}{6}\pi\right)\sin\!\left(ky'-\frac{\pi}{6}\right)\sin(kz')\,\right] e^{-3\,\nu\,k^2\,t}$$

$$\frac{w_1}{U_0} \,=\, \frac{4\sqrt{2}}{3\sqrt{3}}\left[\,\sin\!\left(kz'-\frac{5}{6}\pi\right)\cos\!\left(kx'-\frac{\pi}{6}\right)\sin(ky') - \cos\!\left(ky'-\frac{5}{6}\pi\right)\sin\!\left(kz'-\frac{\pi}{6}\right)\sin(kx')\,\right] e^{-3\,\nu\,k^2\,t}$$

and the dependence on the parameter R is dropped. The reference solution for the family '2' is obtained by reverse the angles $5\pi/6$ and $\pi/6$.

Going back to the original variables, the stagnation points of the above solutions can be calculated by solving the latter system:

$$\sin(kx+\psi) = 0\,, \qquad \sin(ky+\psi) = 0\,. \qquad \sin(kz+\psi) = 0\,, \tag{3.19}$$

Note that both the families share the same positions of the stagnation points and these are placed over the following regular lattice:

$$(x_l,\, y_m,\, z_n) = -\frac{\psi}{k}(1,1,1) - \frac{\pi}{k}(l,m,n)\,, \tag{3.20}$$

where $l,m,n \in \mathbb{Z}$. In the appendix A.1 we provide a linear stability analysis of the stagnation points and prove that they are always unstable equilibria. The above findings do not depend on the parameter R (since this just represents a translation) and the only difference between the two families is the reversal of the stable/unstable manifolds. The same behaviour occurs between the different stagnation points belonging to the same family. As pointed out in Sharma & Sengupta (2019), the presence of unstable equilibria may be the triggering for a period-doubling bifurcation and, subsequently, for a possible transition to the turbulent regime.

3.2. *Examples*

Here we show some plots of the proposed solutions. In particular we display them at the initial time, namely $t = 0$, since the later instants just represent a damping of the initial velocity distribution. We consider dimensionless variables $\boldsymbol{x}^* = \boldsymbol{x}/L$, $\boldsymbol{u}^* = \boldsymbol{u}/U_0$ and $p^* = p/(\rho U_0^2)$ and, without any loss of generality, choose $R = 0$ for both the families. This latter choice is motivated by the necessity of simplifying the graphical representation of the stagnation points in the reference domain, namely the three-dimensional torus $[0,1]^3$.

Figure 1 shows the contours of the fields $\boldsymbol{u}_1^* = (u_1^*, v_1^*, w_1^*)$ (left column) and $\boldsymbol{u}_2^* = (u_2^*, v_2^*, w_2^*)$ (right column) along the planes $x^* = 0.86$, $y^* = 0.86$ and $z^* = 0.08$. The two families display similar patterns for the velocity components even though these show different orientations/angles of the contour lines. We notice that some of these patterns are very close to the two-dimensional Taylor-Green vortex solution (see, for example, the planes at $y^* = 0.86$ and $z^* = 0.08$ of the component v_1^* in the middle left plot).

In figure 2 we show the contours of the pressure fields p_1^* and p_2^* on the same planes. Being the pressure directly related to the kinetic energy and to the enstrophy (i.e. $\|\boldsymbol{\omega}\|^2/2$), we also plot the iso-surfaces for $p_1^* = p_2^* = -0.02$. These highlight the presence of a pattern of Y-shaped structures that identify the regions where the enstrophy and the kinetic energy of the solutions are smaller, that is the regions containing the stagnations points. For $R = 0$ these are obtained by solving the system (3.19) and read:

$$\left(x_l^*,\, y_m^*,\, z_n^*\right) = -\frac{1}{4}(1,1,1) + \frac{1}{2}(l,\, m,\, n) \tag{3.21}$$

where $l,m,n \in \mathbb{Z}$. It is interesting to observe that the Y-shaped structures have different orientations between the two families but "lie" on the same planes, that is planes orthogonal to the direction $(1,1,1)$. The latter is the direction associated with the maximum absolute eigenvalue at the stagnation points, as described in the Appendix A.1.

For the family '1', the left panel of figure 3 shows the streamlines in the neighbourhood of the stagnation points $(1/4, 1/4, 1/4)$ and $(3/4, 3/4, 3/4)$ along with the planes that pass through them and are orthogonal to the direction $(1,1,1)$. Along these planes the contours of the kinetic energy $\|\boldsymbol{u}_1^2\|/2$ are drawn, highlighting the projection of the Y-shaped structures in the neighbourhood of the stagnation points. In the right panel of figure 3 we show the Y-shaped structures along with the iso-surfaces and contours of $\|\mathbb{D}_1^*\|_F^2 = \mathbb{D}_1^* : \mathbb{D}_1^*$ where $\mathbb{D}_1^*$ is the strain-rate tensor (namely the symmetric part of the tensor $\nabla^* \boldsymbol{u}_1^*$) and $\|\cdot\|_F$ denotes the Frobenius matrix norm. The regions where the norm of the strain-rate tensor is close to the maximum value (about 120) appear like

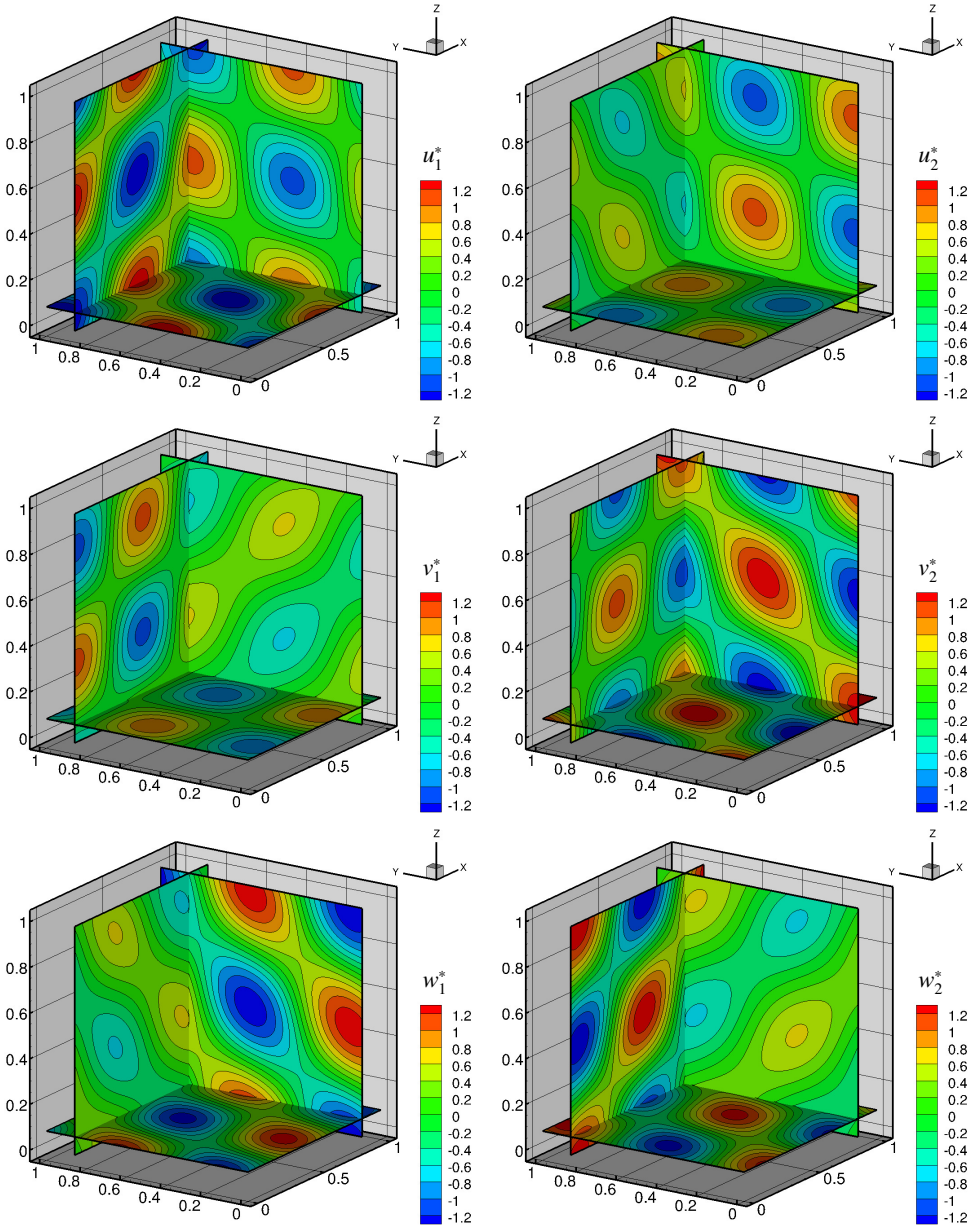

FIGURE 1. Contours of the velocity fields $\boldsymbol{u}_1^*$ (left column) and $\boldsymbol{u}_2^*$ (right column) for $R = 0$ (slices at $x^* = 0.86$, $y^* = 0.86$ and $z^* = 0.08$).

tubular shapes and are approximately oriented along the vector (1, 1, 1), though they are separate from the neighbourhoods of the stagnation points. Note that the maximum of $\|\mathbb{D}_1^*\|_F^2$ is much larger than the enstrophy field (whose maximum is about 0.1). The same behaviour is observed for the family '2' which, therefore, is not displayed here.

As a proof of concept of the possible applications related to the proposed solutions, figure 4 displays the time histories of the averaged kinetic energy per unit of mass [see the equation (3.13)] as predicted by the theoretical solution and by a Finite Volume code (see Di Mascio et al. (2014), Muscari et al. (2017)). In particular, we define the Reynolds number as $Re = U_0 L/\nu$

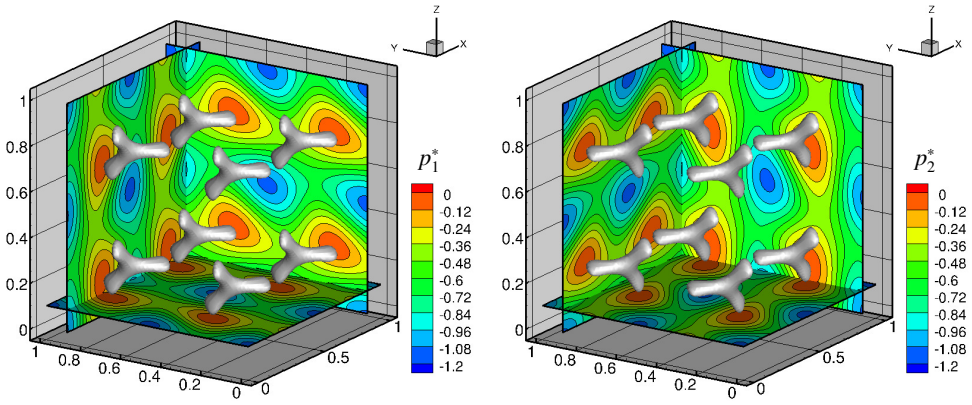

FIGURE 2. Contours of the pressure fields p_1^* (left) and p_2^* (right) for $R = 0$ (slices at $x^* = 0.86$, $y^* = 0.86$ and $z^* = 0.08$) and iso-surfaces at $p_1^* = -0.02$ (left) and $p_2^* = -0.02$ (right).

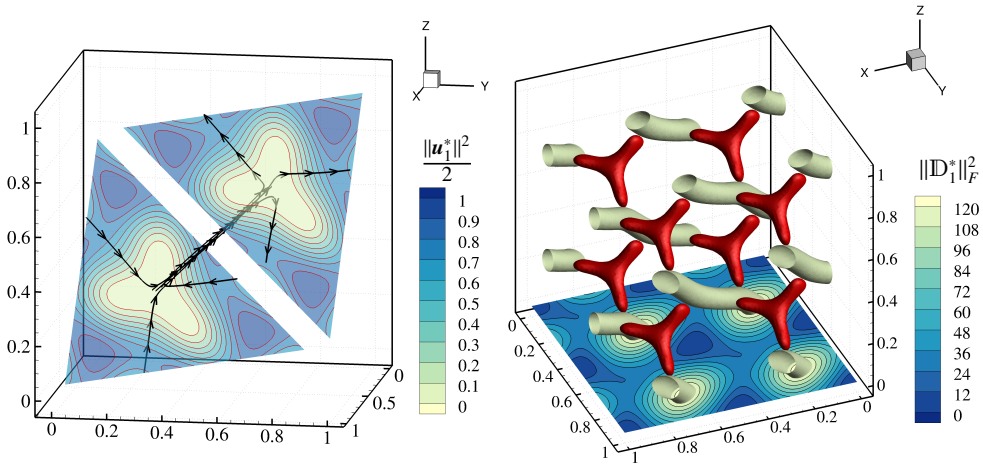

FIGURE 3. Left panel: streamlines close to the stagnation points $(1/4, 1/4, 1/4)$ and $(3/4, 3/4, 3/4)$. Here the planes are orthogonal to the direction $(1, 1, 1)$ and display the contour of the kinetic energy $\|\boldsymbol{u}_1^*\|^2/2$. Right panel: contour of $\|\mathbb{D}_1^*\|_F^2$ on the plane $z^* = 0$ and iso-surface at $\|\mathbb{D}_1^*\|_F^2 = 115$ (here the 'Y'-shaped structures correspond to the iso-surface of the enstrophy at $\|\boldsymbol{\omega}_1^*\|^2/2 = 0.0015$). In both the panels $R = 0$.

and consider the cases $Re = 50$ (left panel of figure 4) and $Re = 1000$ (right panel of the same figure). In both the simulations a uniform grid of 32^3 points has been used. In the former case, the numerical output is practically superimposed to the analytical solution during all the interval of the simulation and this confirms the accuracy of the numerical algorithm. On the contrary, for $Re = 1000$ some instabilities arise at about $t^* = 3$, leading to an increase of dissipation and to a deviation from the theoretical solution. For this latter case, figure 5 displays the evolution of the pressure field along the three coordinate planes at the center of the domain. In particular, the left panel shows the initial pressure field (given by the analytic solution) while the right panel displays the solution at $t^* = 5.6$. At this time instant the breaking down of the analytical vortex pattern and the generation of smaller wave lengths is evident.

The above findings suggest that the proposed solutions may be suited to study the triggering of instabilities and the transition to turbulence in high Reynolds number flows. Further, they may be used for a receptivity/instability analysis based on disturbance enstrophy as described, for

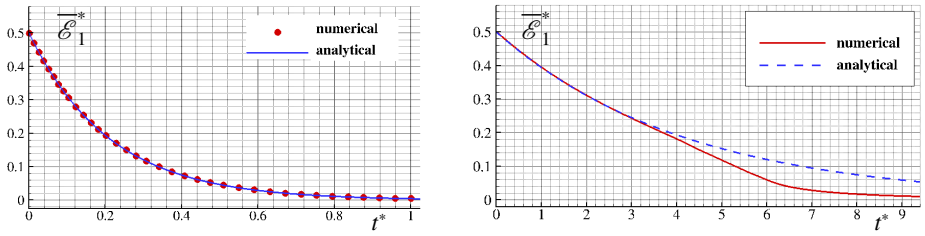

FIGURE 4. Time histories of the averaged kinetic energy per unit of mass for $Re = 50$ (left panel) and $Re = 1000$ (right panel). Comparisons between the analytic solutions and the numerical outputs. In both the panels the solution of the family '1' with $R = 0$ has been used to initialize the computations.

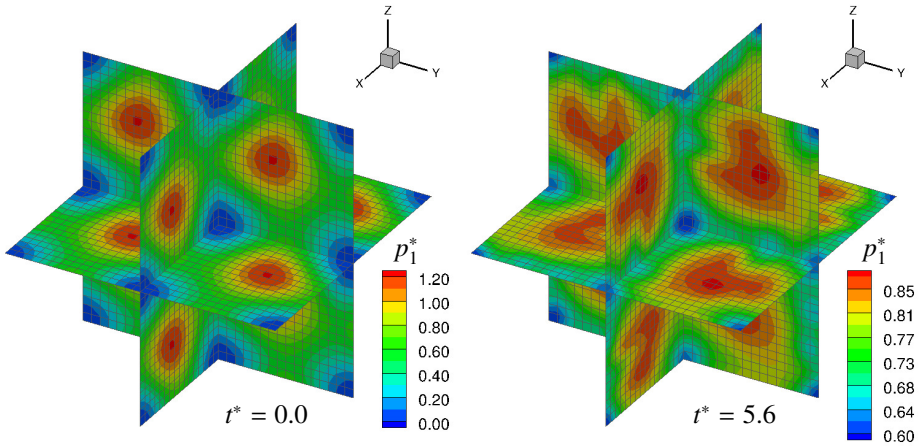

FIGURE 5. Snapshots of the evolution of the pressure field at $Re = 1000$ as predicted by the numerical solver. The analytical solution of the family '1' with $R = 0$ has been used to initialize the computations.

example, in Sengupta et al. (2018b). In any case these topics are beyond the aim of the present work.

4. Some considerations about turbulence

In the introduction and in the previous section we stressed that the proposed solutions may be used to study the onset of instabilities in the laminar flow and the subsequent possible transition to the turbulent regime. This likely occurs for high Reynolds number flows. Conversely, when the Reynolds number is very low, the proposed solutions may be also employed to characterize turbulent flows close to the Kolmogorov micro-scale.

In particular, using the equation (3.13), we define the reference rate of energy dissipation as:

$$\epsilon = \left.\frac{\mathrm{d}\overline{\mathscr{E}}(t)}{\mathrm{d}t}\right|_{t=0} = \nu k^2 U_0^2 , \tag{4.1}$$

where the equality is hereinafter understood as a relation between orders of magnitude (i.e. all numerical values are dropped). Then, defining the Reynolds number as $Re = U_0 L/\nu$, we consider the case $Re = 1$. As a consequence, $U_0 = \nu/L$ and this leads to:

$$\epsilon = k^2 \frac{\nu^3}{L^2} = \frac{\nu^3}{L^4} , \qquad \Rightarrow \qquad L = \left(\frac{\nu^3}{\epsilon}\right)^{1/4} , \tag{4.2}$$

which is exactly the Kolmogorov length scale. The time scale is immediately obtained by setting $T = L/U_0 = L^2/\nu$.

The reason why we discover back the Kolmogorov micro-scale relies in the decomposition described in the Section 2. This implies that all the energy related to the generation of nonlinearities [i.e. the term $(\boldsymbol{u}\cdot\nabla)\,\boldsymbol{u}$] is "absorbed" by the pressure field and gives no contribution to the time derivative $\partial\boldsymbol{u}/\partial t$. Consequently, no smaller length scales are created and, thus, the dynamics is dominated by viscous dissipation. This may probably mean that the flow at the Kolmogorov micro-scale tends to be a Beltrami flow (generalized or not).

Conclusions

Tri-periodic fully 3D analytic solutions of the Navier-Stokes equations have been derived basing on the work of Ethier-Ross & Steinman (1999). These belong to the class of Beltrami's flows and can be gathered in two distinct solutions characterized by positive and negative helicity respectively. In particular, some plots of the proposed solutions have been displayed, showing that these can be regarded as a generalization in three dimensions of the Taylor-Green vortex solution. Further, numerical simulations have been considered in order to illustrate the possible applications related to the theoretical findings.

The proposed solutions are simple to implement and to use for benchmarking numerical codes because, due to their periodicity, there is no need for an explicit modelling of boundaries. Finally, they may be adopted to study the onset of turbulence in high Reynolds number flow, since they represent the free evolution of rotational three-dimensional fluid patterns.

Declaration of Interests

The author reports no conflict of interest.

Acknowledgements

This research was developed within and supported by the MIUR PRIN 2017 Project "FUNdamentals of BREAKing wave-induced boundary dynamics - FUNBREAK", with grant number 20172B7MY9.

Useful discussions with Dr. Andrea Colagrossi, Dr. Salvatore Marrone and Prof. Andrea Di Mascio are gratefully acknowledged. In particular, the author thanks Dr. Salvatore Marrone and Prof. Andrea Di Mascio for the numerical simulations shown in the present paper. Finally, the author dedicates this work to his baby daughter Martina for inspiring him during the sleepless nights.

Appendix A. Details of computation

The substitution of the functions (3.1)-(3.3) in the equations (2.7) and, subsequently, in the equation (2.8) leads to a complex expression made of sines/cosines of the spatial coordinates. This can be regarded as a Fourier series in the variables (x, y, z) containing a finite number of modes whose amplitudes are made of the coefficients A, B, C, D, E, F of the equations (3.1)-(3.3). Since the number of terms in the above expression is huge, the amplitudes of the different modes are obtained by using the standard integral relations of Fourier series through the software Maple for symbolic and numeric computing. Dropping multiple or linear dependent outputs, we

find the following nonlinear system:

$$\begin{cases} B^2C^2FE + A^2D^2FE - B^2CF^2D - AD^2F^2B \\ -A^2CE^2D - AC^2E^2B - 6\,BCFADE = 0\,, \\ \\ -A^2C^2E^2 - BCE^2AD + ADF^2BC - B^2C^2F^2 + A^2D^2E^2 - A^2D^2F^2 \\ +B^2C^2E^2 + BD^2FAE + B^2DFCE - BC^2FAE - A^2DFCE + B^2D^2F^2 = 0\,, \\ \\ A^2D^2F^2 + 2\,A^2DFCE - 2\,BC^2FAE - B^2C^2F^2 \\ -2\,BD^2FAE + B^2C^2E^2 + 2\,B^2DFCE - A^2D^2E^2 = 0\,. \end{cases}$$

Using the software Maple, we find some trivial solutions (which are dropped) and the two families of solutions described in the equation (3.4). Substituting these in the expressions (3.1)-(3.3) and introducing the new parameter $R = F/E$, we find:

$$u = kBDE\left\{\left[\left(\frac{A_{1,2}}{B}\right)\cos(kx) + \sin(kx)\right]\left[-\left(\frac{C_{1,2}}{D}\right)\sin(ky) + \cos(ky)\right][\,\cos(kz) + R\sin(kz)\,]\right.$$
$$\left.-\left[-\left(\frac{A_{1,2}}{B}\right)\sin(kz) + \cos(kz)\right]\left[\left(\frac{C_{1,2}}{D}\right)\cos(kx) + \sin(kx)\right][\,\cos(ky) + R\sin(ky)\,]\right\}e^{-3\,\nu k^2 t}$$

$$v = kBDE\left\{\left[\left(\frac{A_{1,2}}{B}\right)\cos(ky) + \sin(ky)\right]\left[-\left(\frac{C_{1,2}}{D}\right)\sin(kz) + \cos(kz)\right][\,\cos(kx) + R\sin(kx)\,]\right.$$
$$\left.-\left[-\left(\frac{A_{1,2}}{B}\right)\sin(kx) + \cos(kx)\right]\left[\left(\frac{C_{1,2}}{D}\right)\cos(ky) + \sin(ky)\right][\,\cos(kz) + R\sin(kz)\,]\right\}e^{-3\,\nu k^2 t}$$

$$w = kBDE\left\{\left[\left(\frac{A_{1,2}}{B}\right)\cos(kz) + \sin(kz)\right]\left[-\left(\frac{C_{1,2}}{D}\right)\sin(kx) + \cos(kx)\right][\,\cos(ky) + R\sin(ky)\,]\right.$$
$$\left.-\left[-\left(\frac{A_{1,2}}{B}\right)\sin(ky) + \cos(ky)\right]\left[\left(\frac{C_{1,2}}{D}\right)\cos(kz) + \sin(kz)\right][\,\cos(kx) + R\sin(kx)\,]\right\}e^{-3\,\nu k^2 t}$$

where the subscripts '1' and '2' indicate the specific family of the solution and:

$$A_{1,2} = (\,r_{2,1}\,)\,B\,, \qquad C_{1,2} = (\,r_{1,2}\,)\,D\,, \tag{A 1}$$

where:

$$r_1 = \frac{\sqrt{3} - R}{\sqrt{3}\,R + 1}\,, \qquad r_2 = \frac{\sqrt{3} + R}{\sqrt{3}\,R - 1}\,. \tag{A 2}$$

First, we observe that the coefficients B, D and E are redundant and can be replaced by a single parameter $H = k\,BDE$. Further, we highlight that the solution is formally singular for $R = \pm 1/\sqrt{3}$. It is simple to show that such singularities are apparent and can be eliminated by imposing a finite value of the averaged kinetic energy per unity of mass. In particular, we obtain:

$$\overline{\mathscr{E}}(t) = \frac{1}{L^3}\int_0^L\int_0^L\int_0^L \frac{\|\boldsymbol{u}\|^2}{2}\mathrm{d}x\,\mathrm{d}y\,\mathrm{d}z = \frac{27}{4}\,\frac{\left(1+R^2\right)^3}{\left(1-3\,R^2\right)^2}\,e^{-6\,\nu k^2 t}\,H^2 \tag{A 3}$$

We require $\overline{\mathscr{E}}(t)$ at $t = 0$ to be finite and define the reference velocity U_0 such that $\overline{\mathscr{E}}(0) = U_0^2/2$. As a consequence, we obtain the following expression for H:

$$H = \frac{\sqrt{2}}{3\sqrt{3}}\,\frac{\left(1-3\,R^2\right)}{\left(1+R^2\right)^{3/2}}\,U_0\,. \tag{A 4}$$

Substituting the above formula in the equations for $\boldsymbol{u} = (u, v, w)$ and rearranging, we obtain:

$$u_{1,2} = \frac{4\sqrt{2}}{3\sqrt{3}} \{[a_{1,2}\cos(kx) + b_{1,2}\sin(kx)]\,[-c_{1,2}\sin(ky) + d_{1,2}\cos(ky)]\,[e_{1,2}\cos(kz) + f_{1,2}\sin(kz)]$$

$$-\,[-a_{1,2}\sin(kz) + b_{1,2}\cos(kz)]\,[c_{1,2}\cos(kx) + d_{1,2}\sin(kx)]\,[e_{1,2}\cos(ky) + f_{1,2}\sin(ky)]\}\,e^{-3\nu k^2 t}U_0$$

$$v_{1,2} = \frac{4\sqrt{2}}{3\sqrt{3}} \{[a_{1,2}\cos(ky) + b_{1,2}\sin(ky)]\,[-c_{1,2}\sin(kz) + d_{1,2}\cos(kz)]\,[e_{1,2}\cos(kx) + f_{1,2}\sin(kx)]$$

$$-\,[-a_{1,2}\sin(kx) + b_{1,2}\cos(kx)]\,[c_{1,2}\cos(ky) + d_{1,2}\sin(ky)]\,[e_{1,2}\cos(kz) + f_{1,2}\sin(kz)]\}\,e^{-3\nu k^2 t}U_0$$

$$w_{1,2} = \frac{4\sqrt{2}}{3\sqrt{3}} \{[a_{1,2}\cos(kz) + b_{1,2}\sin(kz)]\,[-c_{1,2}\sin(kx) + d_{1,2}\cos(kx)]\,[e_{1,2}\cos(ky) + f_{1,2}\sin(ky)]$$

$$-\,[-a_{1,2}\sin(ky) + b_{1,2}\cos(ky)]\,[c_{1,2}\cos(kz) + d_{1,2}\sin(kz)]\,[e_{1,2}\cos(kx) + f_{1,2}\sin(kx)]\}\,e^{-3\nu k^2 t}U_0$$

where

$$a_1 = -\frac{\sqrt{3}+R}{2\sqrt{1+R^2}}\,, \qquad b_1 = \frac{1-\sqrt{3}R}{2\sqrt{1+R^2}}\,, \qquad c_1 = \frac{\sqrt{3}-R}{2\sqrt{1+R^2}}\,,$$

$$d_1 = \frac{1+\sqrt{3}R}{2\sqrt{1+R^2}}\,, \qquad e_1 = \frac{1}{\sqrt{1+R^2}}\,, \qquad f_1 = \frac{R}{\sqrt{1+R^2}}\,,$$

and $a_2 = c_1$, $b_2 = d_1$, $c_2 = a_1$, $d_2 = b_1$, $e_2 = e_1$, $f_2 = f_1$. Finally, the above coefficients can be rearranged in the form of trigonometric functions as shown in the equations (3.14)-(3.16).

A.1. *Stability of equilibria*

In this section we provide a stability analysis of the stagnation points (equilibria) of the proposed solutions. First, we consider the trajectory of a generic fluid element and introduce the following change of variables:

$$\boldsymbol{u} = \frac{\mathrm{d}\boldsymbol{x}}{\mathrm{d}t} = \frac{\mathrm{d}\boldsymbol{x}}{\mathrm{d}\tau}\frac{\mathrm{d}\tau}{\mathrm{d}t}\,, \qquad \text{with} \quad \frac{\mathrm{d}\tau}{\mathrm{d}t} = \frac{4\sqrt{2}}{3\sqrt{3}}\,e^{-3\nu k^2 t}\,U_0\,, \tag{A 5}$$

and the latter equation, with the additional requirement $\tau(0) = 0$, corresponds to:

$$\tau(t) = \frac{4\sqrt{2}}{9\sqrt{3}\,\nu\,k^2}\left[\,1 - e^{-3\nu k^2 t}\,\right]U_0\,. \tag{A 6}$$

This allows simplifying the equations (3.10)-(3.12) as below:

$$\frac{\mathrm{d}x}{\mathrm{d}\tau} = [\,\sin(kx+\theta)\,\cos(ky+\phi)\sin(kz+\psi) - \cos(kz+\theta)\,\sin(kx+\phi)\sin(ky+\psi)\,] \tag{A 7}$$

$$\frac{\mathrm{d}y}{\mathrm{d}\tau} = [\,\sin(ky+\theta)\,\cos(kz+\phi)\sin(kx+\psi) - \cos(kx+\theta)\,\sin(ky+\phi)\sin(kz+\psi)\,] \tag{A 8}$$

$$\frac{\mathrm{d}z}{\mathrm{d}\tau} = [\,\sin(kz+\theta)\,\cos(kx+\phi)\sin(ky+\psi) - \cos(ky+\theta)\,\sin(kz+\phi)\sin(kx+\psi)\,] \tag{A 9}$$

where the dependence on the specific family of solutions is dropped for the sake of simplicity. To further simplify the analysis, we just focus on the stagnation point $\boldsymbol{x}_0 = (x_0, y_0, z_0) =$

$-\psi/k\,(1,1,1)$, since the results do depend on this specific choice, and consider the following translation $\boldsymbol{x}' = \boldsymbol{x} - \boldsymbol{x}_0$. Expanding in Taylor series around $\boldsymbol{x}' = 0$, we obtain at the leading order:

$$\begin{cases} \dfrac{\mathrm{d}x'}{\mathrm{d}\tau} = k\,(a\,z' + b\,y') \\ \dfrac{\mathrm{d}y'}{\mathrm{d}\tau} = k\,(a\,x' + b\,z') \\ \dfrac{\mathrm{d}z'}{\mathrm{d}\tau} = k\,(a\,y' + b\,x') \end{cases} \tag{A 10}$$

where $a = \sin(\theta-\psi)\cos(\phi-\psi)$ and $b = -\cos(\theta-\psi)\sin(\phi-\psi)$. Substituting the values for $(\theta_{1,2}, \phi_{1,2}, \psi_{1,2})$, we find $a_1 = b_1 = -\sqrt{3}/4$ for the family '1' and $a_2 = b_2 = \sqrt{3}/4$ for the family '2' respectively. This means that the stability of the family '2' close to the point $\boldsymbol{x}_0$ can be obtained from that of the family '1' through a change of sign for the time evolution, that is $t \to -t$. Consistently with the results of the Section §3.1, no dependence on R is observed, since such a parameter just represents a translation of the solution.

For the family '1' the matrix associated with the system (A 10) (apart from the positive multiplicative constant $\sqrt{3}k/4$) is:

$$A = \begin{pmatrix} 0 & -1 & -1 \\ -1 & 0 & -1 \\ -1 & -1 & 0 \end{pmatrix} \tag{A 11}$$

whose eigenvalues are $\lambda_1 = -2$ and $\lambda_2 = \lambda_3 = 1$. The eigenvector associated with λ_1 is $\boldsymbol{v}_1 = (1,1,1)$ while the remaining ones lie on the plane orthogonal to $\boldsymbol{v}_1$. For the family '2' the eigenvalues are opposite in sign, that is $\lambda_1 = 2$ and $\lambda_2 = \lambda_3 = -1$. In both the cases, the equilibrium is unstable, since there always exists a positive eigenvalue. Then, the only difference between the two families is the reversal of the stable/unstable manifolds. Using the relation in the equation (3.20), it is possible to prove that the same occurs between the different stagnation points belonging to the same family.

REFERENCES

Ethier C. Ross & Steinman D.A. 1994 Exact fully 3D Navier–Stokes solutions for benchmarking, *Int. J. Numer. Meth. Fluids*, **19**, 369–375.

Taylor G.I. 1923 LXXV. On the decay of vortices in a viscous fluid, *Philos. Mag.* **46**, 671–674.

Taylor G.I. & Green A.E. 1937 Mechanism of the Production of Small Eddies from Large Ones, *Proc. R. Soc. Lond. A* **158**, 499–521.

Barbato D., Berselli L- C., Grisanti C. R. 2007 Analytical and Numerical Results for the Rational Large Eddy Simulation Model, *J. math. fluid mech.* **9**, 44–74.

Berselli L.C. 2005 On the Large Eddy Simulation of the Taylor–Green vortex, *J. math. fluid mech.* **7**, S164–S191.

Berselli L.C. & Cordoba D. 2009 On the regularity of the solutions to the 3D Navier–Stokes equations: a remark on the role of the helicity, *C. R. Acad. Sci. Paris, Ser. I* **347**, 613–618.

Wang C.Y. 1989 Exact solutions of the unsteady Navier-Stokes equations, *Appl. Mech. Rev.* **42**(11), part 2.

Langlois W.E & Deville M.O. 2014 Slow viscous flow, *Springer International Publishing*, second edition.

Brachet M., Meiron D.I., Orszag S.A., Nickel B.G., Morf R.H., Frisch U. 1983 Small-scale structure of the Taylor-Green vortex, *J. Fluid Mech.* **130**, 411–452.

Drikakis D., Fureby C., Grinstein F.F., Youngs D. 2007 Simulation of transition and turbulence decay in the Taylor–Green vortex, *Journal of Turbulence Volume* **8**(20), 1–12.

Sengupta T.K., Sharma N., Sengupta A. 2018a Non-linear instability analysis of the two-dimensional Navier-Stokes equation: The Taylor-Green vortex problem, *Phys. Fluids* **30**, 054105.

Sengupta, A., Suman, V. K., Sengupta, T. K. and Bhaumik, S. 2018b An enstrophy-based linear and nonlinear receptivity theory *Phys. Fluids* **30**, 054106.

Di Mascio A., Antuono M., Colagrossi A., Marrone S. 2017 Smoothed particle hydrodynamics method from a large eddy simulation perspective, *Physics of Fluids* **29**, 035102.

Sharma N. & Sengupta T.K. 2019 Vorticity dynamics of the three-dimensional Taylor-Green vortex problem, *Physics of Fluids* **31**, 035106.

Goldstein S. 1940 Three-dimensional vortex motion in a viscous fluid, London, Edinburgh Dublin Philos. Mag. J. Sci. **30**(199), 85–102.

Orszag S.A., 1974 Numerical simulation of the Taylor-Green vortex, *Computing Methods in Applied Sciences and Engineering Part 2: International Symposium*, Versailles (Springer, Berlin, Heidelberg, 1974), pp. 50–64.

Muscari, R., Dubbioso, G., Di Mascio, A., 2017 Analysis of the flow field around a rudder in the wake of a simplified marine propeller, *J. Fluid Mech.* **814**, 547–569.

Di Mascio, A., Muscari, R., Dubbioso, G., 2014 On the wake dynamics of a propeller operating in drift. *J. Fluid Mech.* **754**, 263–307.